SYNTHESIS AND CHARACTERIZATION OF $Ti_2(Al_{1-x}, Sn_x)C$ MAX PHASE SOLID SOLUTIONS

An Undergraduate Research Scholars Thesis

by

MARCELL ISTVÁN HARMATI

Submitted to the Undergraduate Research Scholars program at
Texas A&M University
in partial fulfillment of the requirements for the designation as an

UNDERGRADUATE RESEARCH SCHOLAR

Approved by Research Advisor: Dr. Miladin Radovic

May 2018

Major: Mechanical Engineering

TABLE OF CONTENTS

ABSTRACT

Synthesis and Characterization of $Ti_2(Al_{1-x}, Sn_x)C$ MAX Phase Solid Solutions

Marcell István Harmati
Department of Mechanical Engineering
Texas A&M University

Research Advisor: Dr. Miladin Radovic
Department of Materials Science and Engineering
Texas A&M University

MAX phases belong to new family of ternary carbides and nitrides that bridges the gap between the physical and mechanical properties of metals and ceramics. MAX phases have high stiffness, are good thermal and electrical conductors, and have relatively low thermal expansion coefficients, like their binary carbide and nitride counterparts. However, they also have some properties that are more typical of metals, including relatively low hardness, machinability, good thermal shock and oxidation resistance, and damage tolerance. Published reports on the high temperature oxidation and creep resistances of Ti_3SiC_2 and Ti_2AlC indicate that the MAX phases are good candidates for high-temperature applications, such as turbine disk coatings, nuclear fuel cladding, etc. However, it is not yet fully understood to what extent the properties of MAX phases can be tailored by solid solution substitutions or by controlling their microstructure. This research project focuses on the synthesis and characterization of $Ti_2(Al_{1-x}, Sn_x)C$ MAX phase solid solutions, and the effects that alloying with Sn has on the microstructural characteristics and mechanical properties of Ti_2AlC across the solubility range. Synthesis and characterization were performed using various processes and equipment, including spark plasma sintering (SPS), x-ray diffraction (XRD), scanning electron microscopy (SEM), resonant ultrasound spectroscopy (RUS), and Vickers hardness testing, among several refinement methods.

CHAPTER I

INTRODUCTION

MAX phases belong to a new group of ternary carbides and nitrides with the chemical formula $M_{n+1}AX_n$, where M is an early transition metal, A is a group A element, X is carbon or nitrogen, and *n* is 1, 2, or 3 [1]. The crystal structure of MAX phases is a function of *n*, as shown in Figure 1. MAX phases exhibit unusual combinations of properties, and research into their synthesis and characterization has gained significant attention in the last twenty years [1]. As a result, our understanding of these unique materials has progressed dramatically in less than two decades, motivating interest in their potential applications [1].

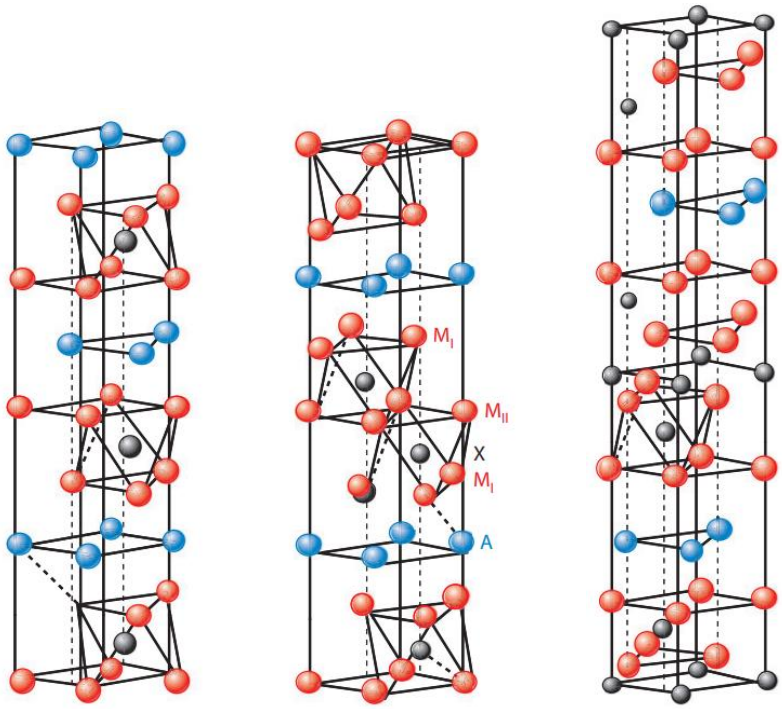

Figure 1: MAX phase unit cells as a function of *n*; (a) 211 (*n* = 1), (b) 312 (*n* = 2), (a) 413 (*n* = 3). Adopted from [9].

Like metallic materials, MAX phases are excellent electrical conductors, with electrical resistivities that typically range from 0.2-0.7 μΩ·m and increase with increasing temperatures [4]. For example, Ti_3SiC_2 and Ti_3SiC_2 conduct electricity better than titanium metal [1]. Similarly to their MX counterparts, MAX phases exhibit good thermal properties, with thermal conductivities between 12-60 W/(m·K) and thermal expansion coefficients (CTE) of 5-10 μK^{-1} [4, 5]. However, with respect to mechanical properties, MAX phases and MX ceramics are noticeably dissimilar. MX ceramics are exceptionally hard, brittle, nonmachinable, damage intolerant, and susceptible to thermal shock [1]. On the other hand, MAX phases have been reported to have Young's and shear moduli of 178-362 GPa and 80-142 GPa, respectively [1,9]. They are also damage tolerant, shock resistant, and easily machinable due to an abundance of mobile basal plane dislocations, which create slip systems along which dislocations can move [1,9, 10]. These slip systems are fewer than that required for polycrystalline ductility – like that in metals – but they allow MAX phases to exhibit pseudoductile behavior [1].

Because of their excellent oxidation resistance and good mechanical properties at high temperatures, MAX phases, especially Ti_2AlC, Cr_2AlC, and Ti_3SiC_2, are being considered for structural and nonstructural high-temperature applications, such as turbine disk coatings, nuclear fuel cladding, etc. [1, 6, 12]. Ti_2AlC, in particular, has a potential for several high-temperature applications due to the relatively low cost of its constituent elemental powders, low density, high oxidation resistance, and crack-healing capabilities [11, 13]. However, though our understanding of the properties and applications of MAX phases has progressed substantially, questions remain regarding the extent to which MAX phases' properties can be tailored using solid solution alloying or by altering their microstructure.

To date, only about 70 pure MAX phases have been synthesized and characterized experimentally. However, by combining more than one element into the M, A, or X sublattices, the number of possible solid solution MAX phases becomes practically infinite. In 2016, Arróyave et al. [3] investigated the intrinsic alloying energies associated with Al-A interactions in the A sublattice of n = 2 or 3 MAX phase systems, where A is Si, P, S, Zn, Ga, Ge, As, Se, Cd, In, Sn, Sb, Te, Hg, Tl, Pb, and Bi [3]. Using density functional theory (DFT), they determined that A-site solid solution alloying, especially for Ti- and Zr-based MAX phases, was possible. Furthermore, Arróyave et al. showed that exothermic interactions exist between Al and Sn, Al and Ge, Al and Sb, and Al and Bi, since the calculated mixing energies were negative [3]. Since the synthesis of quaternary compositions by experimental trial-and-error is effectively unfeasible, Arróyave et al.'s calculations provide a framework for the synthesis of stable (Al, A) solid solution MAX phases.

Only a miniscule portion of the potential solid solutions has been reported, which leaves an incredible amount of opportunities and areas for further exploration and research. A few papers have reported on the mechanical and microstructural properties of solid solutions across the entire solubility range for M-, A-, and C-site substitution [5, 15, 16]. Meng, Zhou, and Wang [15] reported increased Vickers hardness, flexural strength, shear strength, and compressive strength by substituting Ti with V on the M sublattice of the Ti_2AlC MAX phase; Dubois et al. [16] showed by Rietveld refinement that the Ti_3SnC_2 and Ti_3AlC_2 hexagonal unit cell lattice parameters are strongly distorted due to A-site (Al, Sn) solid solutions, and that hardness and Young's modulus increases with increasing Al content; and Barsoum et al. [5] synthesized a $Ti_2Al(C_{0.5,}N_{0.5})$ solid solution that is stronger, harder, and more brittle than Ti_2AlC at room temperature. Furthermore, an even smaller number of papers have investigated the effect of solid

solution alloying on the oxidation resistance of MAX phases [14]. Bei et al. [14] found that as Sn content in a $Ti_2(Al_{1-x}, Sn_x)C$ solid solution increased, oxidation of the A-site elements occurred at a decreasing temperature.

The project outlined in this thesis will systematically explore the effect of varying the composition of alloying elements on the structure and mechanical properties – namely hardness and elastic moduli – of the Ti_2AlC MAX phase. This will be accomplished through the substitution of A-site sublattice points Sn. It is expected that the replacement of Al atoms with larger Sn atoms will increase the Ti-Al bond length in Ti_2AlC and increase the number of vacancy sites on Al. This will result in higher mobility Al atoms, and possibly even better oxidation resistance of Ti_2AlC, while potentially resulting in higher ductility of MAX phase alloys.

CHAPTER II

METHODS

This research project involved the synthesis and characterization of solid solutions on the A-sublattices of the Ti_2AlC MAX phase. A spark plasma sintering (SPS) unit was used to synthesize these solid solutions by reaction-sintering elemental powders into solid ceramic compounds by applying heat – through a pulsed DC current - and pressure. Characterization was performed using x-ray diffraction (XRD), scanning electron microscopy (SEM), resonant ultrasound spectroscopy (RUS), Le Bail and Rietveld refinement, and Vickers hardness testing. These synthesis and characterization methods were carried out using equipment in the Materials Characterization Facility (MCF) in the Frederick E. Giesecke Engineering Research Building and the Materials Development and Characterization Laboratory in the Doherty building.

Synthesis of Ti_2SnC

To determine the temperature at which MAX phases begin to form, and the temperature range at which the sample is the most phase-pure, several samples were synthesized at different temperatures to identify intermediate reactions and phase changes. Temperature levels of 300°C, 500°C, 800°C, 1000°C, 1100°C, and 1250°C were selected based on Zhou et al.'s [7] proposed reaction route of Ti_2SnC. According to Lapauw et al. [17], decomposition of Ti_2SnC begins to occur above 1350°C, so 1250°C was chosen as the maximum reaction sintering temperature.

Ti (99.5% pure, ~325 mesh), Sn (99%, 10 μm), and graphite (99%, 7-10 μm) powders were weighed according to the ratios shown in Table 1. To compensate for material leakage during SPS and carbon deposition from the graphite dies, the following modifications were made to the stoichiometry of the respective powders: Sn: +30%; C: -5%.

Table 1: Powder masses required to synthesize a 5-gram Ti_2SnC sample.

Ti_2SnC	Ti	Sn	C
Atomic Mass (grams/mol)	47.867	118.71	12.0107
Targeted Number of Moles	2	1	1
Corrected Number of Moles	2	1.3	0.95
Molecular Mass (grams/mol)	261.467165		
Correction Factor (5 grams)	0.01912286		
Measured Masses (grams)	1.831	2.951	0.218
Total Mass	5.000		

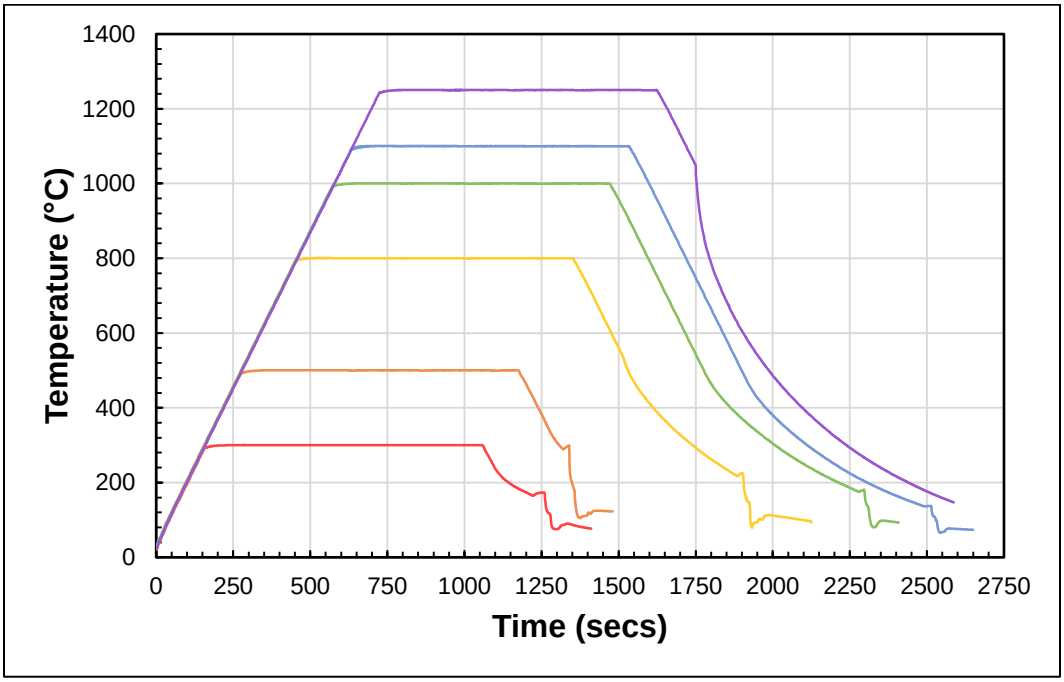

Figure 2: SPS temperature profiles of the six temperature levels for Ti_2SnC synthesis.

The weighed powders were placed in a rotary ball mill and mixed with zirconia pellets for 6 hours at approximately 200 rpm. Then, the mixed powders were separately heated in SPS at a rate of 100°C/min to one of the temperature levels under 5 MPa pressure in Ar. Each final temperature was held for 15 minutes to allow for phase reactions to occur and then ramped down. Figure 2 shows the SPS temperature profiles for the six temperature levels.

Synthesis of $Ti_2(Al_{1-x}, Sn_x)C$

To prepare the $Ti_2(Al_{1-x}, Sn_x)C$ solid solution samples for SPSing, the above-mentioned powders, including Al (99.5%, 7-15 µm), were mixed for the composition range x = 0, 0.2, 0.4, 0.5, 0.6, 0.8, and 1, and were subsequently cold-pressed uniaxially using a stainless-steel die under 30 MPa. Due to less expected leakage of molten A element during SPSing, the adjustments in the stoichiometry were altered for Al and Sn by +0.1 mol. Table 2 shows the powder masses required for a 5-gram $Ti(Al_{1-x},Sn_x)C$ solid solution sample, where x = 0.2.

Table 2: Powder masses required to synthesize a 5-gram $Ti(Al_{0.8},Sn_{0.2})C$ sample.

$Ti(Al_{0.8},Sn_{0.2})C$	**Ti**	**Al**	**Sn**	**C**
Atomic Mass (grams/mol)	47.867	26.981	118.71	12.0107
Targeted Number of Moles	2	0.8	0.2	1
Corrected Number of Moles	2	0.9	0.3	0.95
Molecular Mass (grams/mol)	167.0401			
Correction Factor (5 grams)	0.02993			
Measured Masses (grams)	2.866	0.727	1.066	0.342
Total Mass	5.000			

The SPS heating profile for the composition range was adapted from that reported by Lapauw et al. [17]. A comparison between the temperature profiles of the non-cold-pressed 1250°C Ti_2SnC sample and the cold-pressed $Ti_2(Al_0, Sn_1)C$ sample is shown in Figure 3. Each solid solution sample was heated at a rate of 150°C/min to 500°C under 5 MPa pressure in an Ar atmosphere. After a 2 min dwell, the samples were heated to 1250°C at 100°C/min, then held for 15 mins under 15 MPa pressure. The temperature and pressure were both ramped down quickly after the 15-minute dwell.

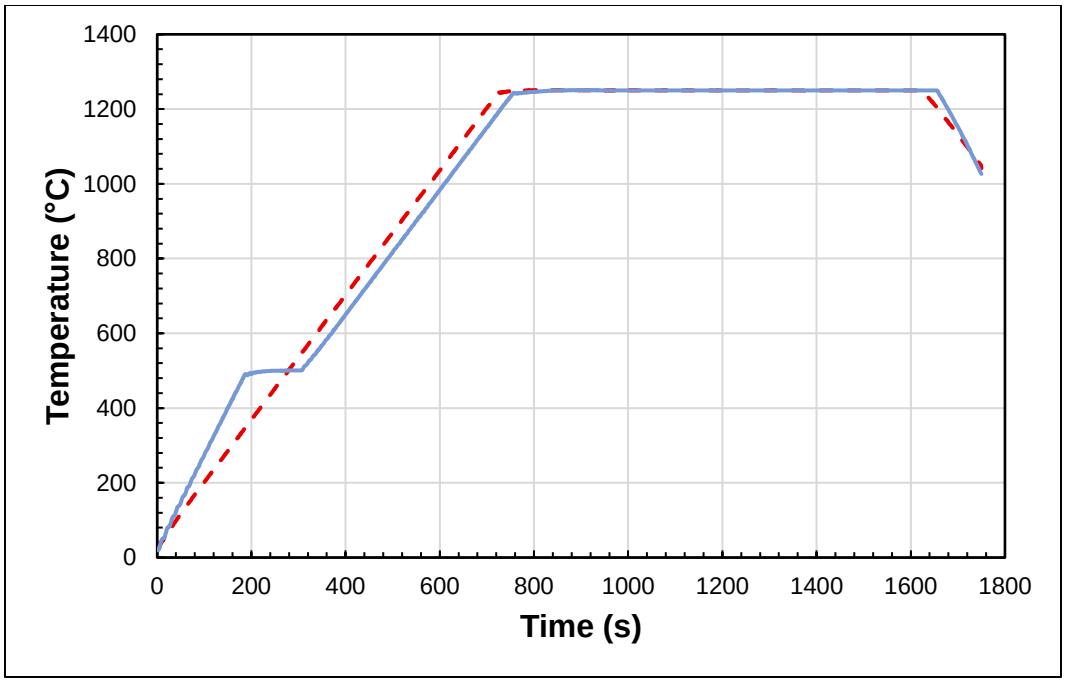

Figure 3: Temperature profiles of the non-cold-pressed 1250°C Ti_2SnC (dashed) and the cold-pressed $Ti_2(Al_{1-x}, Sn_x)C$, where $x = 1$ (solid).

XRD preparation and analysis

The synthesized cylindrical samples were manually grinded using 120 grit sandpaper to remove residual surface impurities, such as graphite or binary carbides, that may have formed at the sample surfaces during the sintering process. X-ray diffraction (Bruker D8 Discover) was performed using Cu Kα radiation at a rate of 3°/min, using a step of 0.05°, from 5° to 70°. Notable diffraction peaks were labeled using EVA software and used to identify intermetallic and/or binary carbide impurities and phases present for the sintered samples. Le Bail and Rietveld refinement were also performed on the composition range samples to determine unit cell lattice parameters and the relative composition of MAX phases and impurities.

Mechanical testing

Elastic constants were determined by resonant ultrasound spectroscopy (RUS) using 2-3 mm thick cylindrical samples. The resonant spectra were collected in a 50-250 kHz range, with a step size of 1 Hz and a one second dwell. The resonant spectra were then de-convoluted by

Quasar RuSpec software to determine the Young's, shear, and bulk moduli, as well as the c11 and c44 elastic constants. Young's and shear moduli are reported. Seven Vickers hardness tests were also carried out for each sample with a different composition, using loading of 300 N.

SEM preparation and analysis

Semicircular slices of the sintered samples were cut from sintered disks using a low-speed saw to create a flat surface for epoxy mounting. The cut samples were placed in a 1-inch mounting cup and lid with a tight seal, and an approximately 4:1 ratio of Epoxicure Resin and Epoxicure Hardener was poured into the cup holding the samples. The epoxy mixture was left until hardened and then removed manually using a press. The 1-inch diameter epoxy cylinder was grinded with progressively finer sandpaper (from 180 to 1200 grit) and subsequently polished using polishing cloths with 3 μm and 0.1 μm diamond suspension and water.

The microstructures of the polished surfaces were analyzed using scanning electron microscopes (SEM – FEI Quanta 600 FEG or JOEL JSM-7500F) equipped with energy dispersive spectroscopy (EDS) with an acceleration voltage of 20kV. Secondary electron imaging was taken of each sample to evaluate its morphology. Backscattered electron (BSE) imaging was also taken, in addition to EDS, and point and area quantitative analysis was used to determine the relative composition of each phase present. Elastic collisions between the accelerated electron beam and atoms in the sample cause electrons to be scattered in the testing chamber and detected by a BSE detector. Heavier elements, such as Sn, have a higher probability of producing elastic collisions, thus result in more backscattered electrons. Conversely, small atoms, such as C, produce fewer backscattered electrons. Therefore, phases with a higher average atomic mass will appear brighter in BSE imaging as more backscattered electrons are detected, allowing different phases to be identified by their apparent brightness. It is important to

note, however, that BSE imaging alone is insufficient for providing quantitative data for the composition of these phases.

On the other hand, EDS can quantify the relative composition of phases present by analyzing the x-rays emitted by the interactions between the accelerated electrons and different atoms in the specimen. The accelerated electron beam excites electrons in the specimen atoms, causing secondary electrons to be released. Electrons from higher energy levels replace the secondary electron, emitting x-rays with wavelengths characteristic of the energy released by the new electron.

CHAPTER III

RESULTS AND DISCUSSION

Synthesis and characterization of Ti_2SnC

Spark plasma sintering

The temperature and displacement (position) profiles of the six Ti, Sn, C powder mixtures sintered at varying temperatures are shown in Figure 4, where the temperature axis shows the temperature recorded by the K-type thermocouple in the SPS vacuum chamber. Similarly, the position axis indicates the position of the vertical hydraulic rams relative to a global datum and is representative of volume changes within the sample.

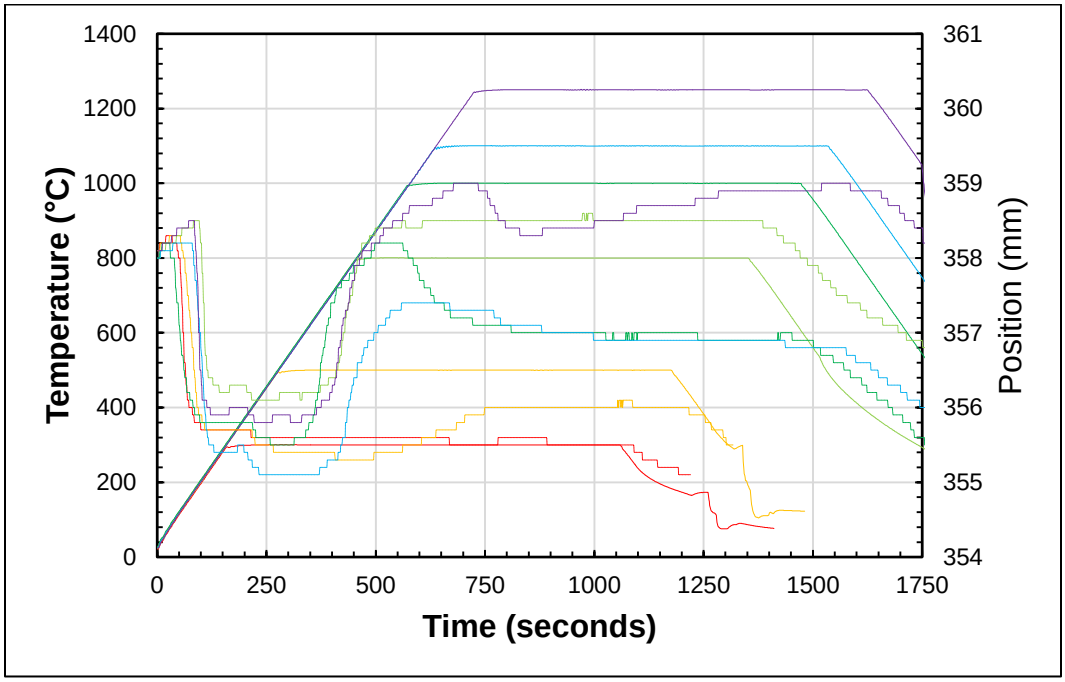

Figure 4: Spark Plasma Sintering Process Parameters. Temperature (solid) and position (dashed) profiles of sintering process of Ti, Sn, and C at 100°C/min temperature increase and 5 MPa pressure.

A decrease in the displacement between the vertical rams indicates a volume decrease in the sintering chamber. In Figure 4, six discrete volume changes can be observed by a relative

position decrease at six different temperatures or temperature ranges. Table 3 details the temperatures at which these volume changes were observed (see below for more details) and descriptions of the possible causes for the volume changes.

Table 3: Observed SPS volume decrease temperature ranges and potential causes.

Key Temperatures	Proposed Cause of Volume Decrease
80-180°C	Lower than melting point of Sn; volume decrease likely due to loose powder settling from application of pressure
360-400°C	Above melting point of Sn; intermetallic formation, as shown by XRD peak identification and EDS
540°C	Formation of Ti_6Sn_5 and Ti_3Sn impurities, indicated by XRD peaks and EDS
980°C	Formation of TiC and Ti_5Sn_3 intermetallics; start of Ti_2SnC MAX phase nucleation, shown by high intensity XRD peak at $2\theta \approx 38°$
1100°C	Ti_2SnC formation; dominant phase, as shown by backscattered electron imaging
1250°C	Intermetallics such as TiC and Ti_6Sn_5 dissolved out; high purity Ti_2SnC

X-ray diffraction

The XRD curves in Figure 5 show characteristic 211 MAX phase peaks ($2\theta \approx 13°$ and 38°) occurring at temperatures of 1000°C and above, indicating that Ti_2SnC is forming. However, while the pure MAX phase appears to begin forming around 1000°C, several intermetallic impurities are found at and above that temperature, reducing the overall phase purity. XRD peaks (Figure 5) and EDS (Figure 6) illustrate that the temperature at which Ti_2SnC forms with small amounts of impurities is approximately 1250°C. As the temperature increases to 1250°C, the distinct Ti_2SnC peaks increase in intensity and impurity peaks, such as those for Ti_6Sn_5 and TiC, decrease in intensity, showing their relative abundance within the sample. This

is in agreement with published results by Zhou et al. [7] Li et al. [8], and Lapauw et al. [17]. Furthermore, the identification of peaks for the temperature range allows for the intermediate phase reactions and intermetallic impurities to be identified, as detailed in Table 4.

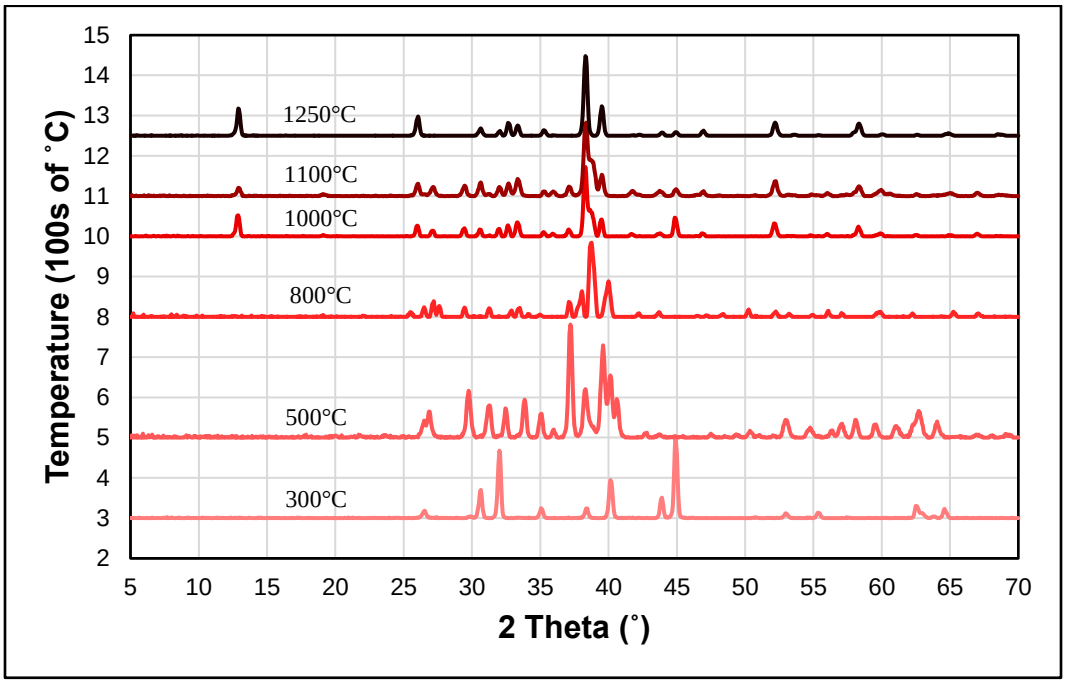

Figure 5: X-ray diffraction curves for the sintered Ti, Sn, C samples at the various temperature levels.

As discussed in Table 3, and as shown in Figure 4, although a volume change is observed below 300°C – indicating a possible reaction – XRD illustrated that at 300°C, only distinct Ti, Sn, and C phases are present. This phenomenon was only seen in the non-cold-pressed samples, showing that the volume change was likely due to loose powder settling as a result of applied pressure by the hydraulic rams in the SPS vacuum chamber and the melting of Sn at 231.9°C.

Scanning electron microscopy

Backscattered electron (BSE) imaging and EDS results allowed for the composition of the phases at each temperature level in the range to be identified, as shown in Figure 6.

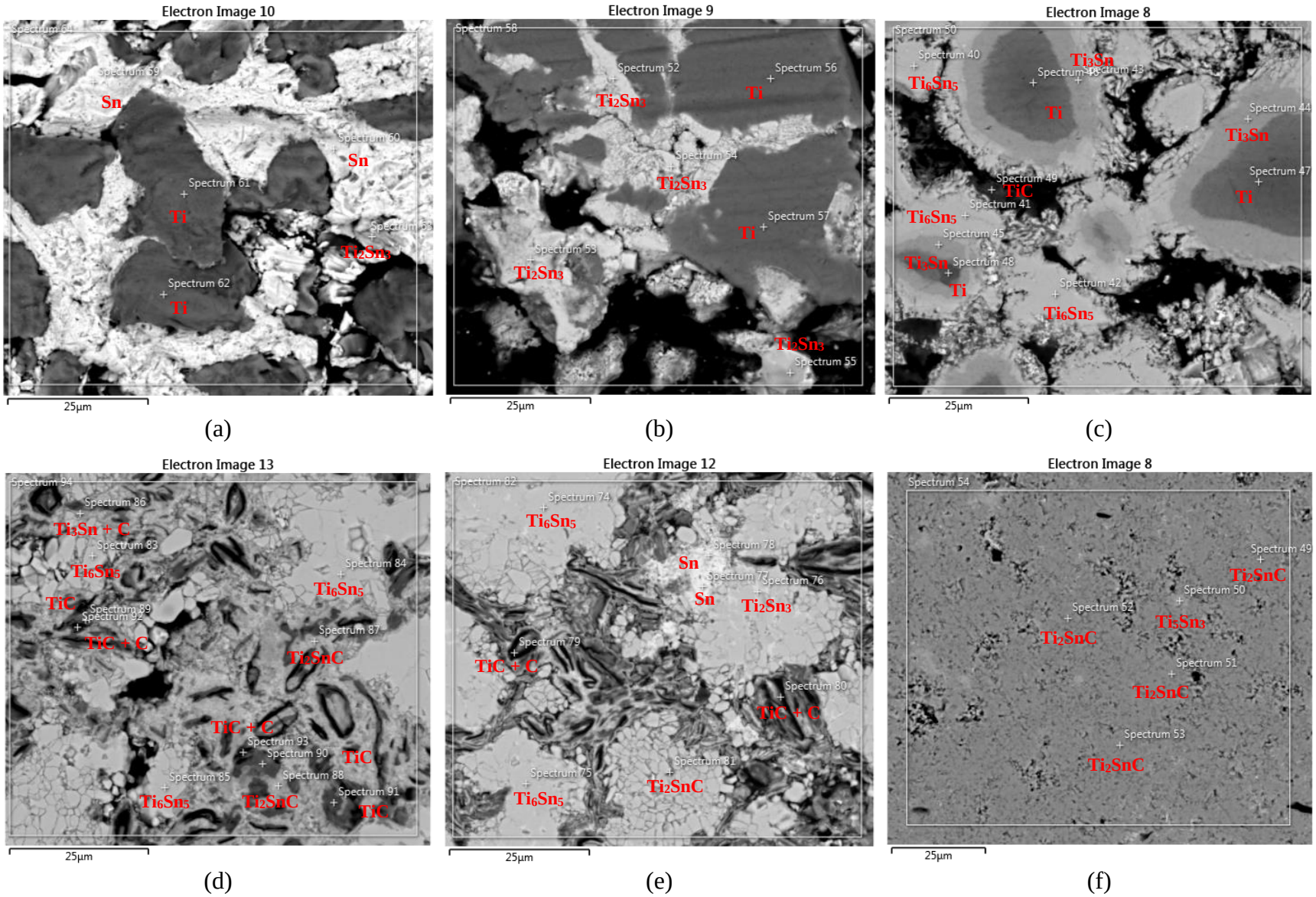

Figure 6: Identified phases from EDS analysis of samples heated to (a) 300°C, (b) 500°C, (c) 800°C, (d) 1000°C, (e) 1100°C, and (f) 1250°C.

It can be seen, in agreement with the XRD curves, that Ti_2SnC begins to form at around 1000°C, though with many impurities. Figure 6 (a-c) show a phenomenon similar to coring during non-equilibrium cooling conditions. This may be a result of excess Sn in the sample resulting in intermetallic phase precipitating in the case of Figure 6 (c), or non-equilibrium cooling after incomplete reactions between various phases. It is clear, however, that the Ti_2SnC at 1250°C is highly phase-pure, as only small amounts of Ti_5Sn_3 were detected from EDS analysis. These results illustrate the importance of selecting appropriate molar ratios and temperatures to achieve optimal synthesis conditions.

Proposed step reactions

Based on the SPS, XRD, and SEM data and imaging, and reported step reactions by Zhou et al. [7], the proposed phase reactions between the temperature range of 300°C to 1250°C are shown in Table 4.

Table 4: Proposed phase reactions of Ti, Sn, and C between the temperature range of 300-1250°C.

Temperature Range	**Identified Phase Reactions**
~25°C to 300°C	$Sn(s) \rightarrow Sn(l)$
300°C to 500°C	$2Ti(s) + 3Sn(l) \rightarrow Ti_2Sn_3(s)$
500°C to 800°C	$5Ti_2Sn_3(s) + 8Ti(s) \rightarrow 3Ti_6Sn_5(s)$ $Ti_6Sn_5(s) + 9Ti(s) \rightarrow 5Ti_3Sn(s)$
800°C to 1000°C	$Ti(s) + C(s) \rightarrow TiC(s)$ $Ti_6Sn_5(s) + 4TiC(s) + C(s) \rightarrow 5Ti_2SnC(s)$
1000°C to 1100°C	$Ti_6Sn_5(s) + 4Sn(l) \rightarrow 3Ti_2Sn_3(s)$ $Ti_6Sn_5(s) + 2Ti_3Sn(s) + 6C(s) \rightarrow 6Ti_2SnC(s)$
1100°C to 1250°C	$Ti_6Sn_5(s) + 4TiC(s) + C(s) \rightarrow 5Ti_2SnC(s)$ $Ti_2Sn_3(s) + 3Ti(s) \rightarrow Ti_5Sn_3(s)$

Synthesis and characterization of $Ti_2(Al_{1-x},Sn_x)C$

X-ray diffraction

The XRD curves for the $Ti_2(Al_{1-x}, Sn_x)C$ samples are shown in Figure 7. Peak identification showed that both Ti_2SnC and Ti_2AlC peaks were present for $0.8 \leq x \leq 0.2$, though those of Ti_2SnC were higher than those of Ti_2AlC. Previous experiments showed that a final temperature of 1400°C produced the most phase-pure Ti_2AlC samples. However, since the final sintering temperature of the solid solution MAX phases was not adjusted according to composition, solid solutions with higher Al content ($x < 0.5$) did not produce high intensity characteristic 211 MAX phase peaks at $2\theta \approx 13°$. Conversely, near-optimal synthesis conditions were created for solid solutions with higher Sn content ($x > 0.6$), resulting in large 211 peaks.

More Al intermetallic phases were also observed by peak identification for $0.8 \leq x \leq 0.2$, indicating that excess Al was present in the samples; some excess Sn was detected for $x \geq 0.5$.

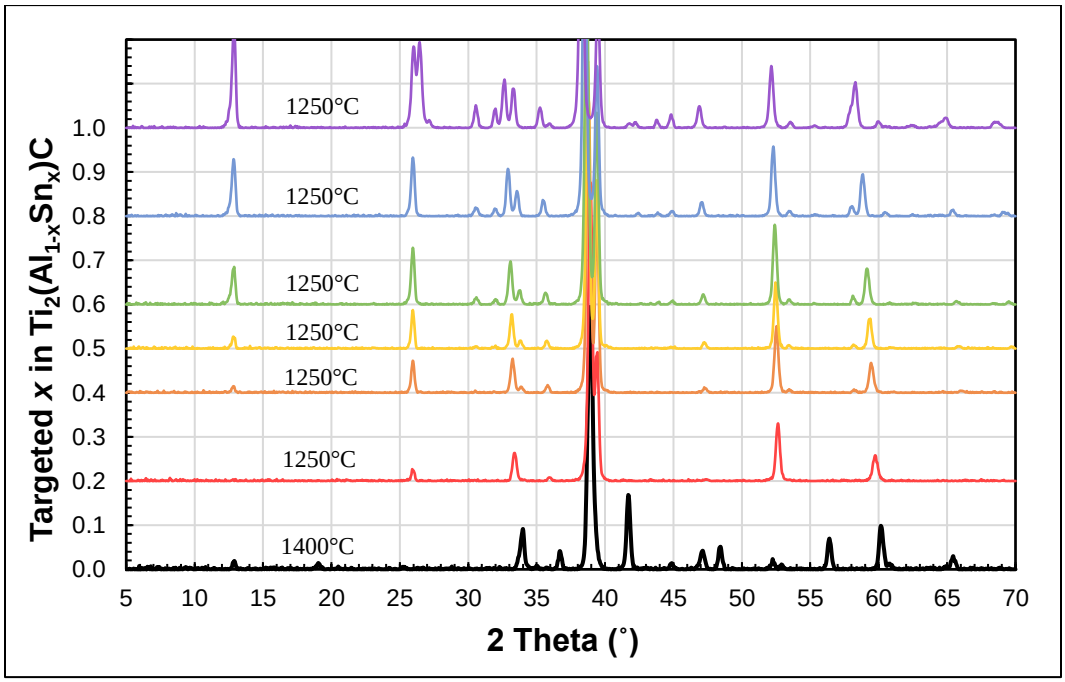

Figure 7: Diffraction peaks of $Ti_2(Al_{1-x}, Sn_x)C$ MAX phase solid solutions for $0 \leq x \leq 1.0$.

By refining previously known lattice parameters for Ti_2SnC and Ti_2AlC unit cells using the Le Bail method, the a and c lattice parameters of the $Ti_2(Al_{1-x}, Sn_x)C$ were found. As shown in Figure 8, the height of the unit cell, denoted by the c lattice parameter, is effectively independent of the Sn content in the MAX phase solid solution. The c lattice parameter was not expected to increase significantly due to the layered structure of the MAX phases, as shown in Figure 1. On the other hand, the a lattice parameter increases linearly from 3.079 Å (x = 0) to 3.164 Å (x = 1.0), which is indicative of a Ti-Al bond length increase, as predicted, due to the substitution of larger Sn atoms into the Al sites. The a and c lattice parameters found by Le Bail refinement for Ti_2AlC, 3.164 Å and 13.684 Å, respectively, are in agreement with those reported by Kanoun, Goumri-Said, and Reshak [2] and Hug [21].

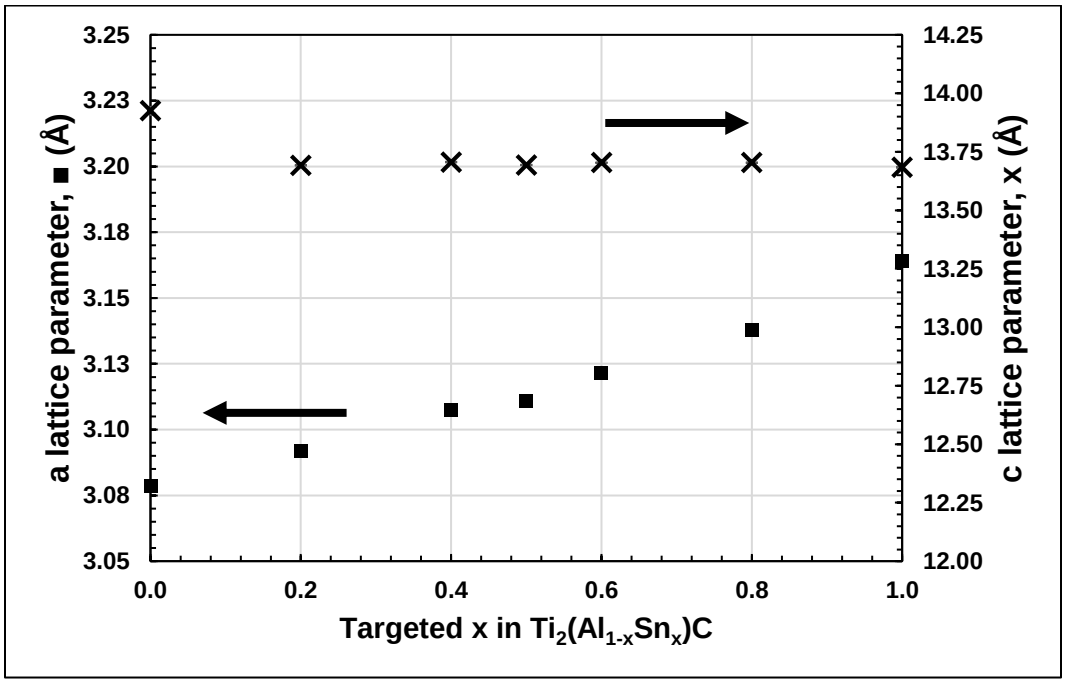

Figure 8: Lattice parameters a and c of $Ti_2(Al_{1-x}, Sn_x)C$ MAX phase unit cell for $0 \leq x \leq 1.0$.

Rietveld refinement of the solid solution samples for the different compositions showed MAX phase purity of between 85-95%, as shown in Figure 9. The primary impurities, as indicated by Rietveld, were TiC, $TiAl_x$, and $TiSn_x$. There appears to be no correlation between the abundance of purities and the value of *x*, indicating that the impurities may be a result of non-ideal synthesis conditions. These conditions may include excess A element from powder mixing or non-optimal maximum reaction sintering temperatures, as previously discussed. By fine-tuning the composition and maximum SPSing temperature of the solid solution MAX phases, higher purity bulk samples may be achieved.

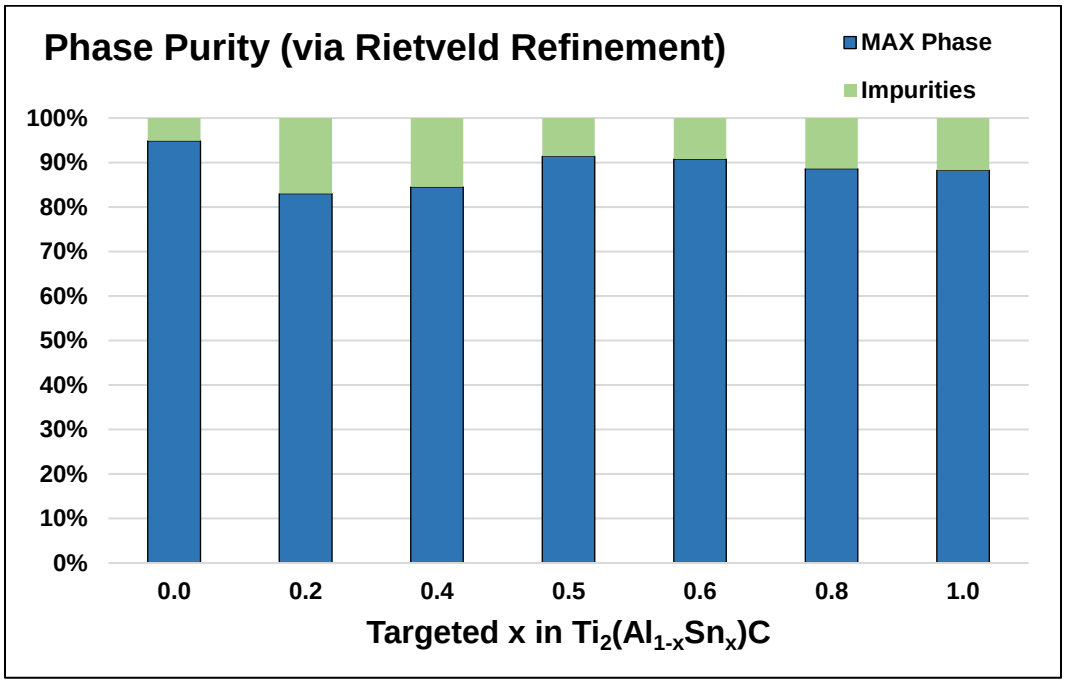

Figure 9: Relative 211 MAX phase purity of bulk $Ti_2(Al_{1-x}, Sn_x)C$ samples for $0 \leq x \leq 1.0$.

Scanning electron microscopy

EDS analysis of a $Ti_2(Al_0, Sn_1)C$ sample with identified phases is shown Figure 10. The pre-compressed samples appear to be more dense than the non-cold-pressed samples of the different temperature levels. Spectrum 35 of EDS also shows that the average composition of the area scanned has a Ti:Sn:C molar ratio of 1.85:1:0.98, which is almost exactly that for Ti_2SnC.

The other spectra illustrate the intermetallic and binary carbide impurities present in the sintered sample. The backscatter image shown for the $Ti_2(Al_0, Sn_1)C$ sample and Rietveld compositional (Figure 9) analysis suggests the excess Sn is present in the sample. As previously discussed, slight modifications to the ratio of mixed powders would further increase phase purity in the sintered samples.

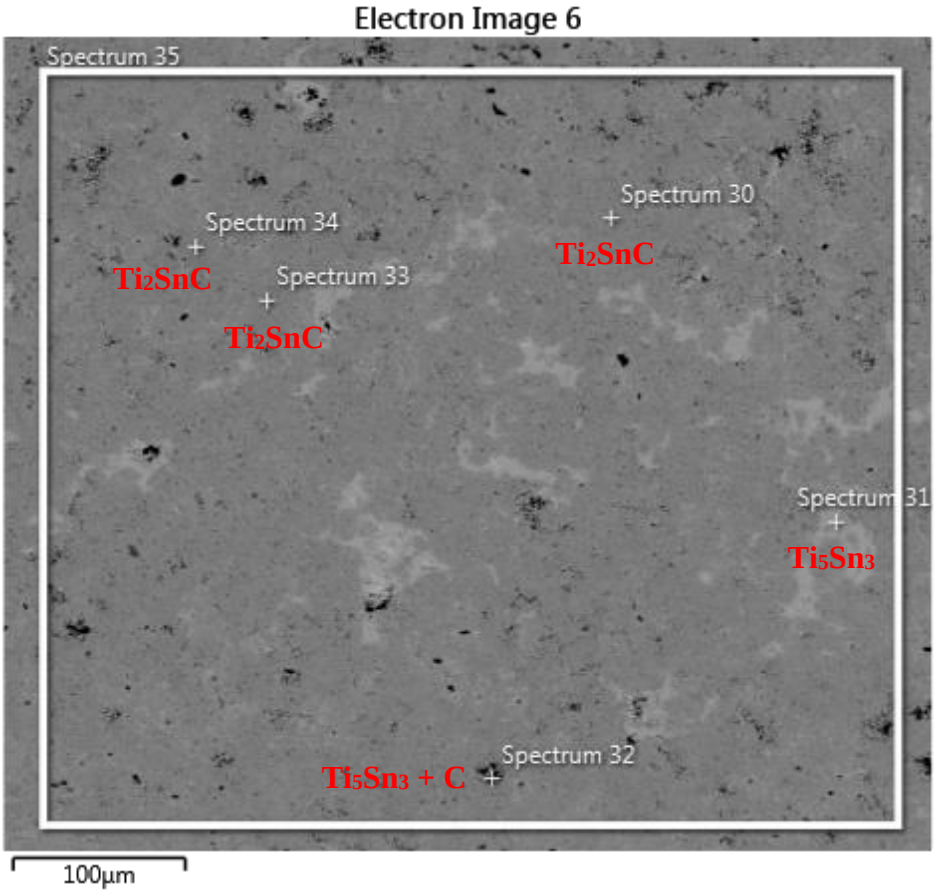

Figure 10: Identified phases from EDS analysis of cold-pressed $Ti_2(Al_0, Sn_1)C$ sample.

Mechanical properties

The Young's and shear moduli of the $Ti_2(Al_{1-x}, Sn_x)C$ composition range are plotted in Figure 11. The Young's moduli for Ti_2AlC (x = 0) and Ti_2SnC (x = 1.0) were found to be 241.8 GPa and 263.3 GPa, respectively. Ching et al. [18] reported theoretical Young's moduli of 262.2 GPa and 216.5 GPa for Ti_2AlC and Ti_2SnC, respectively, showing relatively good agreement

with experimental results presented here. Kanoun, Goumri-Said, and Reshak [2] calculated the Young's modulus of Ti_2SnC, using density functional theory (DFT), to be 293.3 GPa. Barsoum's and Radovic's [9] experimental values for the Young's modulus of Ti_2AlC (E = 277 GPa) are also in good agreement with these results. The Young's moduli of the samples appear to increase slightly with increasing *x*, but the rms error is too high to confidently state that the differences were not due to random errors. It was expected that the Young's moduli would increase from that of Ti_2AlC as *x* increased due to solid solution strengthening and decrease as $x \rightarrow 1.0$.

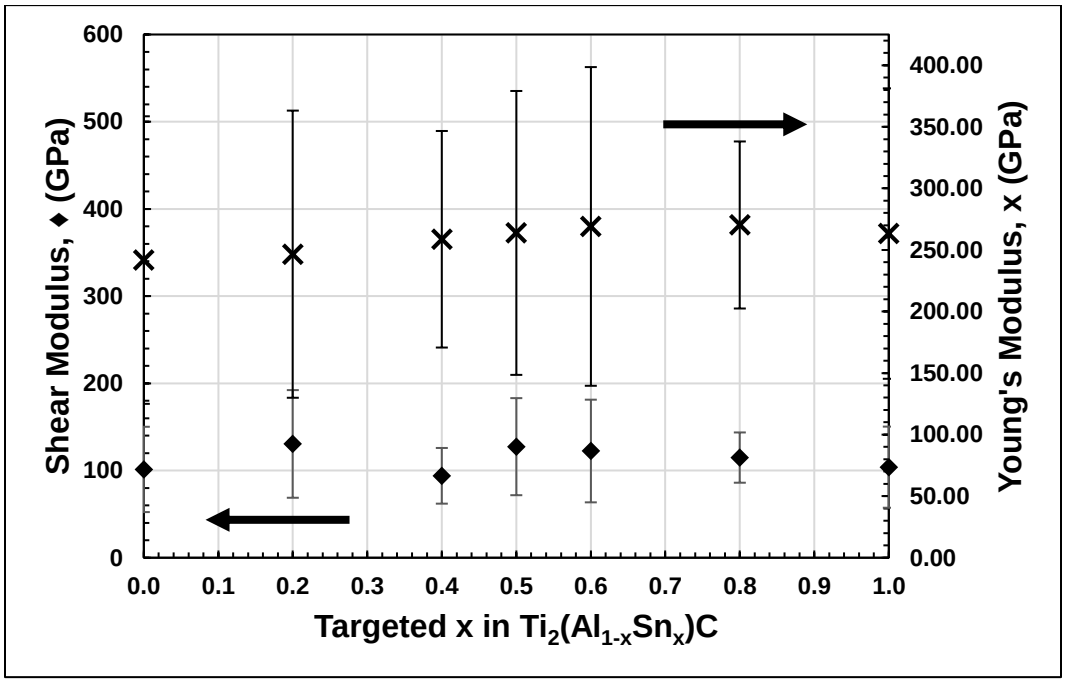

Figure 11: Young's and shear moduli of $Ti_2(Al_{1-x}, Sn_x)C$ MAX phase solid solutions for $0 \leq x \leq 1.0$, found by resonant ultrasound spectroscopy.

The shear moduli for Ti_2AlC and Ti_2SnC were found to be 101.3 GPa and 103.8 GPa, respectively, which is within the margin of error to align with Ching et al.'s [18] theoretical values. Barsoum and Radovic [9] reported a shear modulus of 118 GPa for Ti_2AlC, which is also

in agreement with these results. Results for the different compositions indicate no relationship between *x* and shear modulus, however the error bars are too large to accurately report on this.

The average Vickers hardness values for the range of compositions are shown in Figure 12. Hardness appears to decrease from 4.27 GPa to 2.41 GPa as *x* increases, with a large decrease beginning at $x = 0.6$. Barsoum, Brodkin, and El-Raghy [20] reported a Vickers hardness of 5.5 GPa for Ti_2AlC, higher than these results. Zhou et al. [7] and Barsoum and Yaroschuk [19] reported hardness values of 3.7 GPa and 3.5 GPa, respectively, for Ti_2SnC which, although higher than these results, still indicates a negative correlation between hardness and *x*.

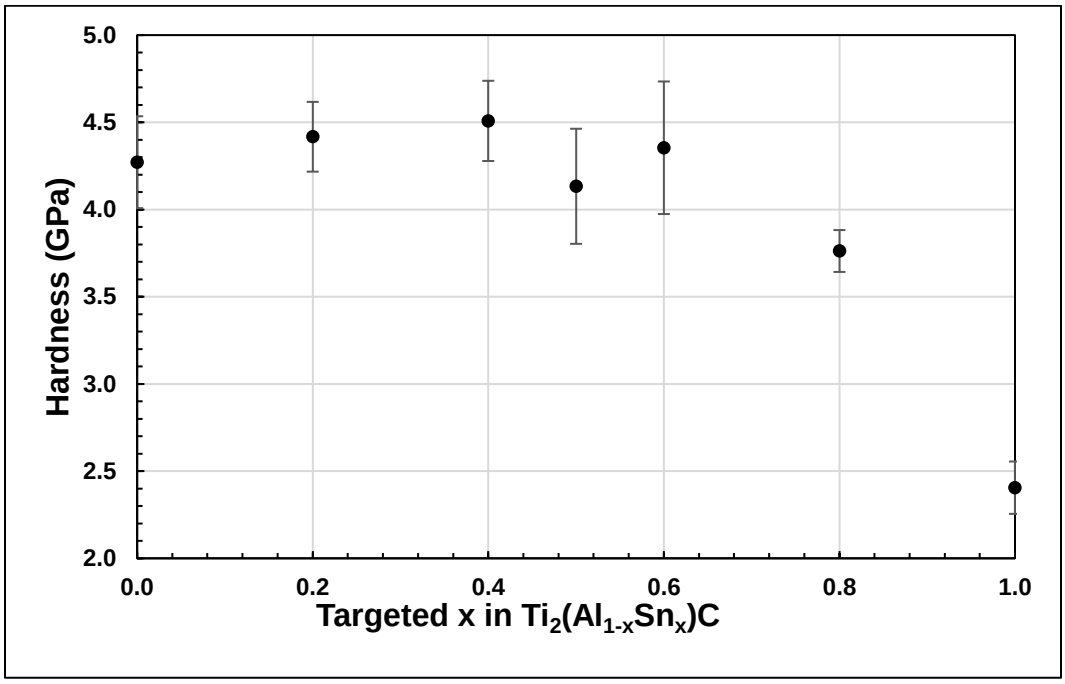

Figure 12: Vickers hardness of $Ti_2(Al_{1-x}, Sn_x)C$ MAX phase solid solutions for $0 \leq x \leq 1.0$ under 300 N loading.

CHAPTER IV

CONCLUSION

- Ti_2SnC begins forming at 1000°C but is of low phase-purity; at 1250°C it is the dominant phase and has only a small amount of Ti_5Sn_3 intermetallic phases
- No reactions take place below 300°C; volume changes due to settling powder in non-cold-pressed samples and melting of Sn at approximately 231.9°C
- Excess Al and Sn impurities formed with composition range, as shown by XRD; less extra powder needed to compensate for leakage during SPS
- Coring between 800°C and 1100°C seems to occur, possibly due to excess A-element or non-equilibrium cooling after incomplete reactions
- Ti_2SnC and Ti_2AlC diffraction peaks were both present for $0.8 \leq x \leq 0.2$, indicating successful synthesis of A-site solid solution MAX phases
- Not adjusting maximum sintering temperatures to account for compositional differences may result in non-ideal synthesis conditions and fewer targeted or expected phases
- Slight positive correlation between E and x, possibly due to solid solution strengthening, Rms error is too large to accurately determine relationship; no correlation may exist
- Shear moduli found to be independent of Sn content in solid solution MAX phase
- Hardness decreases non-linearly with increasing Sn content
- Le Bail refinement shows linear increase in a lattice parameter, likely due to increased Ti-Al bond length; no apparent change in c lattice parameter
- Rietveld refinement shows 85-95% purity, improvable by optimal synthesis conditions
- SEM shows the cold-pressed samples are more dense than non-cold-pressed samples

CHAPTER V

FUTURE WORK

Future work with regard to this research will involve the synthesis and characterization of other MAX phases, such as Ti_2GeC, Ti_2SbC, and Ti_2BiC, to find the optimal synthesis parameters for high-purity bulk samples. A-sublattice solid solutions with Al will also be synthesized and characterized with the above Group XIV and XV elements. This future work will explore the feasibility of tailoring the mechanical properties and oxidation resistance of MAX phase solid solutions, and their potential applications.

REFERENCES

[1] Radovic, M., & Barsoum, M. W. (2013). MAX phases: bridging the gap between metals and ceramics. *American Ceramics Society Bulletin*, *92*(3), 20-27.

[2] Kanoun, M. B., Goumri-Said, S., & Reshak, A. H. (2009). Theoretical study of mechanical, electronic, chemical bonding and optical properties of Ti_2SnC, Zr_2SnC, Hf_2SnC and Nb_2SnC. *Computational Materials Science*, *47*(2), 491-500.

[3] Arróyave, R., Talapatra, A., Duong, T., Son, W., Gao, H., & Radovic, M. (2017). Does aluminum play well with others? Intrinsic Al-A alloying behavior in 211/312 MAX phases. *Materials Research Letters*, *5*(3), 170-178.

[4] Barsoum, M. W. (2013). *MAX phases: properties of machinable ternary carbides and nitrides*. John Wiley & Sons.

[5] Barsoum, M. W., El-Raghy, T., & Ali, M. (2000). Processing and characterization of Ti_2AlC, Ti_2AlN, and $Ti_2AlC_{0.5}C_{0.5}$. *Metallurgical and Materials Transactions A*, *31*(7), 1857-1865.

[6] Smialek, J. L., & Garg, A. (2014). Microstructure and oxidation of a MAX phase/superalloy hybrid interface.

[7] Zhou, Y., Dong, H., Wang, X., & Yan, C. (2002). Preparation of Ti_2SnC by solid—liquid reaction synthesis and simultaneous densification method. *Materials Research Innovations*, *6*(5-6), 219-225.

[8] Li, Z. Y., Wang, L. B., Zhong, G. C., Li, S. S., & Zhou, A. G. (2014). Synthesis of Porous Ti_2SnC from TiH_2-Sn-TiC/Graphite Powders in Tube Furnace. In *Key Engineering Materials* (Vol. 602, pp. 130-133). Trans Tech Publications.

[9] Barsoum, M. W., & Radovic, M. (2011). Elastic and mechanical properties of the MAX phases. *Annual review of materials research*, *41*, 195-227.

[10] Farber, L. (1999). Transmission electron microscopy study of a low-angle boundary in plastically deformed Ti_3SiC_2. *Philosophical magazine letters*, *79*(4), 163-170.

[11] Song, G. M., Pei, Y. T., Sloof, W. G., Li, S. B., De Hosson, J. T. M., & Van der Zwaag, S. (2008). Oxidation-induced crack healing in Ti_3AlC_2 ceramics. *Scripta Materialia*, *58*(1), 13-16.

[12] Hoffman, E. N., Vinson, D. W., Sindelar, R. L., Tallman, D. J., Kohse, G., & Barsoum, M. W. (2012). MAX phase carbides and nitrides: Properties for future nuclear power plant in-core applications and neutron transmutation analysis. *Nuclear Engineering and Design*, *244*, 17-24.

[13] Wang, X. H., & Zhou, Y. C. (2003). High-temperature oxidation behavior of Ti_2AlC in air. *Oxidation of Metals*, *59*(3-4), 303-320.

[14] Bei, G., Pedimonte, B. J., Fey, T., & Greil, P. (2013). Oxidation behavior of MAX phase $Ti_2Al_{(1-x)}Sn_xC$ solid solution. *Journal of the American Ceramic Society*, *96*(5), 1359-1362.

[15] Meng, F. L., Zhou, Y. C., & Wang, J. Y. (2005). Strengthening of Ti_2AlC by substituting Ti with V. *Scripta materialia*, *53*(12), 1369-1372.

[16] Dubois, S., Bei, G. P., Tromas, C., Gauthier-Brunet, V., & Gadaud, P. (2010). Synthesis, microstructure, and mechanical properties of $Ti_3Sn_{(1-x)}Al_xC_2$ MAX phase solid solutions. *International Journal of Applied Ceramic Technology*, *7*(6), 719-729.

[17] Lapauw, T., Vanmeensel, K., Lambrinou, K., & Vleugels, J. (2015). Rapid synthesis and elastic properties of fine-grained Ti_2SnC produced by spark plasma sintering. *Journal of Alloys and Compounds*, *631*, 72-76.

[18] Ching, W. Y., Mo, Y., Aryal, S., & Rulis, P. (2013). Intrinsic Mechanical Properties of 20 MAX-Phase Compounds. *Journal of the American Ceramic Society*, *96*(7), 2292-2297.

[19] Barsoum, M. W., Yaroschuk, G., & Tyagi, S. (1997). Fabrication and characterization of M_2SnC (M= Ti, Zr, Hf and Nb). *Scripta materialia*, *37*(10), 1583-1591.

[20] Barsoum, M. W., Brodkin, D., & El-Raghy, T. (1997). Layered machinable ceramics for high temperature applications. *Scripta Materialia*, *36*(5), 535-541.

[21] Hug, G. (2006). Electronic structures of and composition gaps among the ternary carbides Ti_2MC. *Physical Review B*, *74*(18), 184113.